Optimal sensor selection for sensor-based sorting based on automated mineralogy data

Marius Kern [a, *], Laura Tusa [a], Thomas Leißner [b], Karl Gerald van den Boogaart [a], Jens Gutzmer [a]

[a] Helmholtz-Zentrum Dresden-Rossendorf, Helmholtz Institute Freiberg for Resource Technology, Chemnitzer Straße 40, 09599, Freiberg, Germany
[b] Institute of Mechanical Process Engineering and Mineral Processing, Technical University Bergakademie Freiberg, Agricolastraße 1, 09599, Freiberg, Germany

ABSTRACT

Assessing the success of sensor-based sorting in the raw materials industry currently requires time-consuming and expensive empirical test work. In this contribution we illustrate the prospects of successful sensor selection based on data acquired by scanning electron microscopy-based image analysis. Quantitative mineralogical and textural data from more than 100 thin sections were taken to capture mineralogical and textural variability of two different ore types from the Hämmerlein Sn–In–Zn deposit, Germany. Parameters such as mineral grain sizes distribution, modal mineralogy, mineral area and mineral density distribution were used to simulate the prospects of sensor-based sorting using different sensors. The results illustrate that the abundance of rock-forming chlorite and/or density anomalies may well be used as proxies for the abundance of cassiterite, the main ore mineral. This suggests that sorting of the Hämmerlein ore may well be achieved by either using a short-wavelength infrared detector — to quantify the abundance of chlorite — or a dual-energy X-ray transmission detector to determine the abundance of cassiterite. Empirical tests conducted using commercially available short-wave infrared and dual-energy X-ray transmission sensor systems are in excellent agreement with simulation-based predictions and confirm the potential of the novel approach introduced here.

© 2019 Published by Elsevier Ltd.

1. Introduction

Sensor-based sorting is a technology applied by the mining industry to reject coarse barren particles (in a size range between 10 and 100 mm) of a heterogeneous ore at an early stage of a beneficiation process (Knapp et al., 2014; Wills and Finch, 2016; Wotruba and Harbeck, 2010). The sorting process can be subdivided into four basic steps, as illustrated in Fig. 1 by the example of a chute sorter (Nienhaus et al., 2014). Before sensor-based sorting can be implemented into a flow sheet it must be the first objective to identify the sensor, which is able to detect — or even quantify — a suitable property that allows classifying the particles of the investigated ore type into concentrate and waste. Most commonly, direct identification of the mineral of interest is not possible because suitable sensors are not available. In such cases, a measureable property that correlates well with the mineral/element of interest — a so-called

proxy — can be selected for sensor-based sorting. Examples of commonly-detected properties/proxies are atomic density with a (dual-energy) X-ray transmission sensor, (DE-)XRT for short (e.g. Neubert and Wotruba (2016); Robben et al. (2013); Walker (2017)), color, fluorescence, or transparency (optical sensor), short-wavelength infrared or near-infrared radiation (SWIR/NIR; e.g. Dalm et al. (2017); Phiri et al. (2018); Iyakwari et al. (2013)), or X-ray fluorescence (XRF; e.g. Nadolski et al. (2018)).

The state-of-art approach to find a suitable sensor for sorting a particular raw material is to carry out repeated and varied trial-and-error batch tests (e.g., Nienhaus et al., 2014; Wotruba and Harbeck, 2010), leaving a high potential for optimization. This classical approach requires several steps. First, a sorting parameter (e.g. color) and a matching sensor (→ optical sensor), suitable to separate ore from waste must be chosen based on qualitative evaluation of the ore. This step is followed by lab-scale batch tests with 10–100 ore particles (e.g., Neubert and Wotruba, 2016; Riedel and Dehler, 2010; Robben et al., 2013). Based on the results of such lab-scale batch tests a suitable sensor is identified and test work
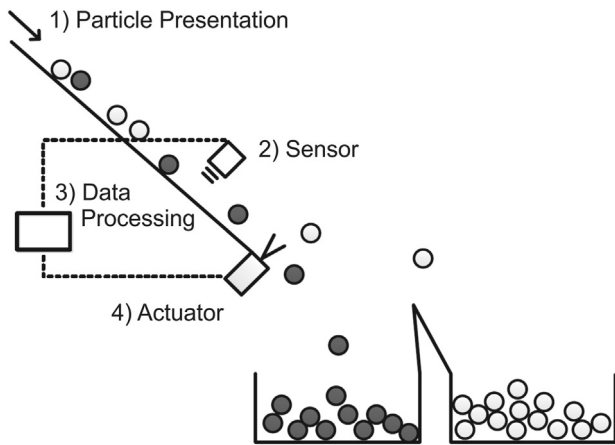
Fig. 1. Schematic drawing of a sensor based chute sorter (modified from Nienhaus et al. (2014)). (1) After optional conditioning with water, single particles are presented on a chute. (2) The particles are examined contact-free with a sensor detecting tangible particle properties. (3) An electronic processing unit evaluates the obtained information and forwards it to (4) an actuator, which ejects particles with specific characteristics from the material stream.

continues on a pilot plant scale. It is during the latter pilot tests that bulk assay data are used to assess sorting performance in terms of, e.g., recovery, grade and mass pull. The latter terms are obvious prerequisites for a cost-benefit assessment to decide whether a sensor-based sorter should be implemented in an industrial operation.

It is obvious that a prior knowledge of the raw material to be sorted limited to a qualitative description and bulk chemical assay data is insufficient. For example, it is not clear why a number of ore particles is rejected ($\rightarrow$ waste), and vice versa, why a number of particles is transferred into the concentrate. It is also unclear whether the tested sorting mechanism functioned to its full potential or if it is possible to improve the sorting performance. Furthermore, there are no indications whether parameter(s) other than those selected for empirical test work could be used to concentrate the element/mineral more efficiently.

It is an intuitive expectation that a more comprehensive understanding of mineralogical and textural characteristics of the raw material to be sorted will provide prior insight into the effectiveness of a sorting process that is based on physical characteristics set by the minerals that constitute the ore. The data needed can be provided by scanning-electron microscopy energy-dispersive X-ray spectroscopy (SEM-EDS)-based image analysis (a.k.a. automated mineralogy, Fandrich et al., 2007). In this study, automated mineralogy data is used in a novel approach of simulating the success of sorting — without the need of extensive empirical test work. Quantitative mineralogical and microfabric data obtained on a set of polished sections provide the suitable fundament to simulate the performance of sensor-based sorting with a selection of different separation parameters. The polymetallic Hämmerlein deposit (Erzgebirge, Germany), a skarn-greisen orebody with cassiterite (SnO_2) mineralization (particle sizes between 5 μm and 3 mm) serves as a case study to illustrate this novel approach. Simulation-based results are validated by actual sorting tests using two different sensor systems that are commercially available.

2. Materials and methods

The samples used in this study originate from the $+590$ m level of the Hämmerlein deposit which can be accessed via the visitors' mine *Besucherbergwerk Zinnkammern Pöhla*. Hand specimens were collected for various studies concerning the different lithounits, ore

types, and host rocks (e.g. Kästner, 2016; Miehlbradt, 2017; Richter, 2016; Winkler, 2017). Whilst the samples are regarded as being representative of the area of the mine that was accessible to sampling, they may not necessarily be representative for the entire deposit.

2.1. The Hämmerlein deposit

The polymetallic Hämmerlein deposit is located in the central portion of the Erzgebirge of the Free State of Saxony, Germany, close to the border to Czech Republic (Fig. 2) and is currently explored by Saxore Bergbau GmbH. The deposit comprises of two lithologically distinct parts: a Sn−In−Zn skarn (skarn ore) and greisenized mica schist known as Schiefererz (Schuppan and Hiller, 2012). The main commodity of economic interest in the Hämmerlein deposit is Sn contained in the mineral cassiterite (SnO_2). Grain sizes of cassiterite range between 5 μm and 3 mm in the skarn ore and 0.1−3 mm in the Schiefererz. Zn and In, both contained in sphalerite (ZnS) (Bauer et al., 2017) are regarded as important by-products (Treliver Minerals Limited, 2015). Economically significant tin mineralization in the skarn ore is related to a late metasomatic overprint expressed by the mineral assemblage cassiterite-chlorite-fluorite-sulfides (Kern et al., 2018a). This assemblage occurs in irregular pods, lenses and veins (Fig. 3 A). The preferred association between cassiterite and chlorite, as well as fluorite and sulfide minerals can readily be quantified (Kern et al., 2018a). The skarn ore is surrounded by extensively altered and locally greisenized mica schist (Schiefererz) (Miehlbradt, 2017). In immediate contact with the skarn, 1−2 cm thick cassiterite-bearing veinlets can be found crosscutting the mica schist (Fig. 3 B).

2.2. Sample preparation

Hand specimens were cut to blocks of approximately $4.2 \times 2.4 \times 0.5$ cm size. A thin slice of each block was sawed off to prepare a polished section of either 30 μm or 150 μm thickness and lateral dimensions of 4.2×2.4 cm. Although sensor-based sorting is usually applied to irregularly shaped particles instead of rectangular cuboids with a flat surface and straight edges, we approached

Fig. 2. Location of the Hämmerlein deposit in Germany.
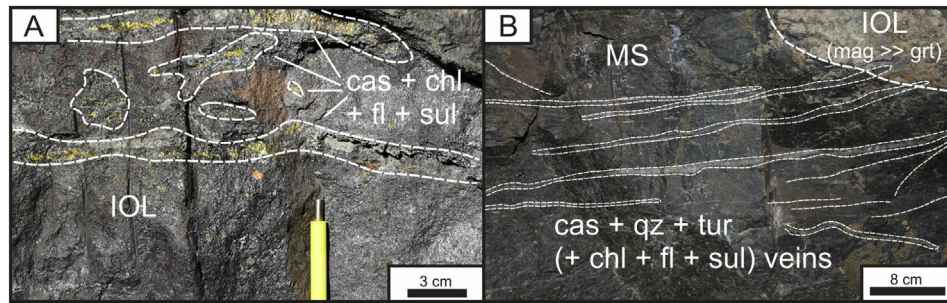
Fig. 3. Two photographs of the cassiterite mineralization (CM) in skarn and mica schist (Schiefererz, MS). A. Assemblage of cassiterite, chlorite, fluorite, and the sulfide minerals chalcopyrite, arsenopyrite and pyrite overprint the iron oxide lithounit (IOL) forming pods and lenses. B. Numerous quartz- and cassiterite-bearing veinlets crosscut the MS (= *Schiefererz*) and reach into the skarn (IOL with mag ≫ grt). Abbreviations: IOL = Iron oxide lithounit; MS = mica schist, cas = cassiterite, chl = chlorite, fl = fluorite, sul = sulfide, mag = magnetite, grt = garnet, qz = quartz, tur = tourmaline. From Kern et al. (2018a).

the hypothesis that the impact of this obvious difference in particle shape is limited because of the small mineral grain sizes and strong mineral intergrowth typical for skarn ore and Schiefererz.

A total of 101 sets (a set consisting of a block and the corresponding polished section) were selected from the two ore types skarn (n = 81) and Schiefererz (n = 20). All analyzed samples from the different ore types and lithounits (as introduced by Kern et al. (2018a)) are listed in Table 1. A threshold of 0.1 wt % Sn in cassiterite per sample was chosen as a first pass to distinguish between ore and waste rock. This simple threshold is exceeded by 35 % of the skarn samples (28 out of 81) and 60 % of the Schiefererz samples (12 out of 20). The threshold is lower than the economic cut-off grade for mining (0.5 wt % total Sn; see Treliver Minerals Limited (2015)) but regarded as reasonable at the sorting stage, where the ore has only been blasted, transported and crushed (personal communication Dr. Marco Roscher, Saxore Bergbau GmbH).

2.3. Mineral liberation analysis

Quantitative mineralogical analyses with the modified approach for automated mineralogy by Kern et al. (2018b) were conducted on the entire set of polished sections using a Mineral Liberation Analyzer (MLA; from FEI Company, Hillsboro, OR, USA). A FEI Quanta 650 F field-emission scanning-electron microscope (FE-SEM; from FEI Company, Hillsboro, OR, USA) equipped with two Bruker Quantax X-Flash 5030 energy-dispersive X-ray (EDX) detectors (from Bruker Company, Billerica, MA, USA) was used. The SEM was operated at an acceleration voltage of 25 kV and a probe current of 10 nA. Grain-based X-ray mapping (GXMAP) discriminates minerals by their grayscale and uses a closely spaced grid of

X-ray points to map the surface of the polished sections. In this measurement mode, the surface of the polished section is subdivided into square frames. MLA measurement conditions were set to a pixel size of 2 or 3 μm (for fine-grained or coarse-grained samples, respectively) at a step size of 6 × 6 and an acquisition time of 5 ms. The side length of a frame varied between 1 and 1.5 mm (geometric mean = 1.3 mm). The software MLALookUP (Krupko et al., 2018) and MLA Suite 3.1.4 from FEI were used for data processing. Results include particle maps as well as modal mineralogy, mineral area (2-dimensional equivalent to volume), particle density, mineral grain size distribution and mineral associations (Fandrich et al., 2007; Gu, 2003).

In addition, the average density of each image frame was calculated by multiplying the density of each detected mineral with the mineral abundance within the frame. The frame with the highest density (= *highest-density frame*; HDF) is regarded as a suitable proxy because samples with local anomalies of high density are likely to contain cassiterite—the mineral with the highest density in the Hämmerlein ore.

2.4. Short-wavelength infrared spectroscopy

Hyperspectral SWIR data from block samples was acquired using a SisuROCK drill-core scanner equipped with an AisaFENIX hyperspectral sensor (both from SPECIM, Spectral Imaging Ltd., Oulu, Finland). A scanning speed of 25.06 mm/s, a frame rate of 15 fps and an integration time of 4 s were used. The spatial resolution of the resulting hyperspectral scans is 1.7 mm/pixel. In the relevant range of the SWIR region for the current study (1800–2300 nm) the spectral resolution is 12 nm.

Table 1
Ore types and lithounits (as introduced by Kern et al. (2018a)) of studied samples with Sn contained in cassiterite above and below the threshold of 0.1 wt % (defined by Mineral Liberation Analysis). Cassiterite mineralization is related to an assemblage of cassiterite-chlorite-fluorite-sulfides. Note that samples that consist entirely of this characteristic mineral assemblage may still have a content of Sn in cassiterite below 0.1 wt %.

Lithounit	≥0.1 wt % Sn in cassiterite	<0.1 wt % Sn in cassiterite	Total
Skarn			
Feldspar-pyroxene-epidote lithounit (FPEL)	1	5	6
Garnet lithounit (GL)	3	14	17
Amphibole lithounit (AL)	5	7	12
Iron oxide lithounit (IOL)	12	15	27
Sphalerite mineralization (SM)	1	2	3
Cassiterite mineralization (CM)	6	3	9
Gneiss (GS)	0	7	7
Total	28	53	81
Schiefererz			
Total	12	8	20

The samples were measured three times and the scans were averaged after the pre-processing consisting of sensor shift and geometric correction of the lens effect using the MEPHySTo toolbox (Jakob et al., 2017). Further data processing was performed using the ENVI version 5.1 (Exelis Visual Information Solutions, Boulder, CO, USA) software. The resulted averaged scan was subjected to spectral smoothing using the savgol filter.

Chlorites from Hämmerlein have an intermediate Fe–Mg composition with slight variations (Fe-rich vs. Mg-rich). In the SWIR region of the electromagnetic spectrum, the main intermediate chlorite absorption feature is located at 2252 nm very close with the main epidote feature (Pontual et al., 1997). The effect of the epidote feature at 2252 nm was reduced by subtracting its specific secondary feature at 1831 nm (Pontual et al., 1997). The resulting chlorite abundance map of the blocks was processed and analyzed in MATLAB R2015b (MathWorks, Inc., Natlick, MA, USA) to calculate the average gray level of each block. The obtained value is considered an indicator for chlorite abundance in the sample.

2.5. Dual energy X-ray transmission

DE-XRT uses broad-band radiation from an X-ray tube. The radiation penetrates the material to be sorted while it is moved along the scanning area (von Ketelhodt and Bergmann, 2010). The material attenuates the received X-ray radiation and thereby decreases the modulation amplitude of the sensor. The degree of attenuation depends on the atomic density and the thickness of the material (von Ketelhodt and Bergmann, 2010). Two channels of the X-ray sensor capture different energy levels, which allow the characterization of the material by its atomic density and almost regardless of its thickness. The resulting gray-scale image shows fractions of high (dark) and low (light) atomic density (Riedel and Dehler, 2010).

In this study a HI-RAY 10 DE-XRT sensor (Smiths Detection Inc., Watford, United Kingdom) was run at 160 kV. Higher energy levels were achieved by applying a metal foil in front of the sensor that filtered low kV radiation. The conveyor belt speed was set to 2.8 m/s at an acquisition time of 1.25 ms/frame with a resulting resolution of approximately 1.2×3.5 mm.

3. Results

3.1. Ore characteristics

Iron oxide minerals (magnetite, hematite), silicates (amphibole, garnet and chlorite) and sulfide minerals dominate the mineralogy of the skarn. Cassiterite concentrations vary between 0.0 and 19.2 wt % (average of Ø 0.6 wt %). The Schiefererz, in contrast, consists of quartz, feldspar and mica with cassiterite contents between 0.0 and 11.9 wt % (Ø 2.1 wt %). Sample variability is visualized by ten selected samples from different lithounits and ore types. Fig. 4 shows false-color images created from data sets of the applied methods. A table with results from analyses with MLA (modal mineralogy, mineral area, highest-density frame, mineral grain size distribution), SWIR (chlorite area) and DE-XRT (frame with the highest density) can be found in the electronic supplementary (Table 1. Skarn ore; Table 2. Schiefererz).

3.2. Simulations

Data from automated mineralogy enables the simulation of a theoretically unlimited number of sorting experiments. Upgrading curves based on the cassiterite content and three proxies (chlorite area, highest-density frame and fluorite grain size) are discussed in the following chapters. The simulated results from sorting by

chlorite area and highest-density frame are compared to experiments with commercially available sorting equipment (SWIR and DE-XRT, respectively).

3.2.1. Cassiterite content

The upgrading curves in Fig. 5 A and B (skarn ore) are described in detail to inform the interpretation of Fig. 5 C and D (Schiefererz) as well as Fig. 6, Fig. 7 and Fig. 8, which have a similar layout. General reviews on upgrading curves can be found in Drzymała (2006, 2007, 2008).

Fig. 5 A plots a *Fürstenau-II diagram* (e.g. Drzymała, 2006) with gangue recovery (x-Axis) against cassiterite recovery (y-Axis) for the case that all samples are sorted according to the property cassiterite content (wt %). The first sample sorted to the concentrate is the one with the highest cassiterite content (19.2 wt %), followed by the sample with the second highest cassiterite content (11.8 wt %), *et cetera*. Recovery of 99 % cassiterite is reached with sample 39 out of 81. Each of the remaining 42 samples contains less than 0.1 wt % Sn in cassiterite. The curve is labeled with selected threshold values of cassiterite that is recovered at a specific recovery/mass pull ratio. For example, at 85 % cassiterite recovery and 20 % gangue recovery, all samples with ≥ 1 wt % cassiterite are classified as concentrate. The upgrading curve would touch (or cross) the diagonal line (labeled *no upgrading*) if gangue recovery and cassiterite recovery was identical.

Fig. 5 B shows the *technical efficiency-recovery diagram* as introduced by Finch and Gomez (1989). The cassiterite recovery (x-axis) is plotted against the technical efficiency (= cassiterite recovery − gangue recovery) on the y-axis. The technical efficiency is a parameter that allows assessment of separation performance and defines an ideal threshold value. The diagonal marks ideal upgrading.

Fig. 5 C shows the Fürstenau-II diagram and Fig. 5 D the technical efficiency-recovery curve for Schiefererz. According to the data sets, it is possible to recover 95% cassiterite and reject 60 % of the gangue. The technical efficiency reaches values > 60 %.

To reach a recovery of more than 80 % cassiterite from skarn ore or Schiefererz, a sensor that identifies cassiterite (or tin) at concentrations between 1 and 2 wt % in a fast and precise manner would be necessary. To the best knowledge of the authors this is not possible with state-of-the-art sensor technology. Nevertheless, the upgrading curves yield important information as they show the *mineralogical barrier* for sorting. This ideal sorting result can be reached in theory, but not in practice for an unlimited amount of samples — no matter how efficient the applied proxy is. The mineralogical barrier is displayed in Figs. 6,7 and 8, for orientation. Any positive sorting result plots between the mineralogical barrier and the *diagonal of no upgrading*. An efficient upgrading curve approximates to the mineralogical barrier.

3.2.2. Chlorite area

The area of chlorite from MLA data is compared to the data set acquired by SWIR. Good agreement between both methods is inferred from the upgrading curves (Fig. 6A and B). The chlorite proxy shows technical efficiency of up to 45 % for cassiterite recovery of 70 % — while 75 % of the gangue is rejected. The SWIR identified chlorite of 1 area % and less without problems, which qualifies for a cassiterite recovery of over 90 %.

The technical efficiency between 0 and 20 % cassiterite recovery is below 10 %. This means that the samples with the highest chlorite area are not particularly rich in cassiterite. Reason is the presence of two chlorite varieties with only slightly different chemical signatures (Fe-rich vs. Mg-rich; see Kern et al. (2018a)).

The chlorite area in the Schiefererz is only 1 % in average. Consequently, the proxy shows limited technical efficiency in MLA
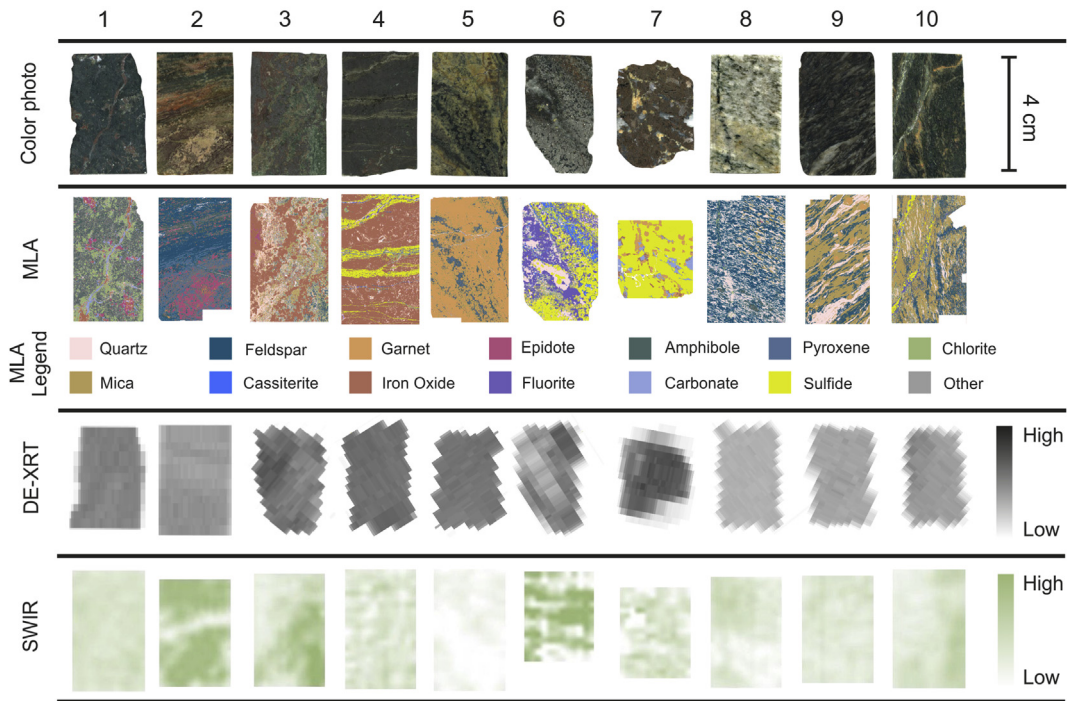
Fig. 4. Selected samples from the Hämmerlein deposit illustrating mineralogical and microfabric diversity (From left to right: 1 = Amphibole lithounit, 2 = Feldspar-pyroxene-epidote lithounit, 3 = Iron oxide lithounit, 4 = Iron oxide lithounit with cassiterite mineralization, 5 = Garnet lithounit, 6 = Cassiterite mineralization, 7 = Sphalerite mineralization, 8 = Gneiss, 9 = Mica schist, 10 = Schiefererz). From top to bottom each sample is shown as a color photo, a false-color image compiled from MLA data showing spatial distribution of minerals, a gray-scale image compiled from DE-XRT data showing areas of high density (dark) and a false-color image compiled from SWIR data showing areas of high chlorite abundance (green). (For interpretation of the references to color in this figure legend, the reader is referred to the Web version of this article.)
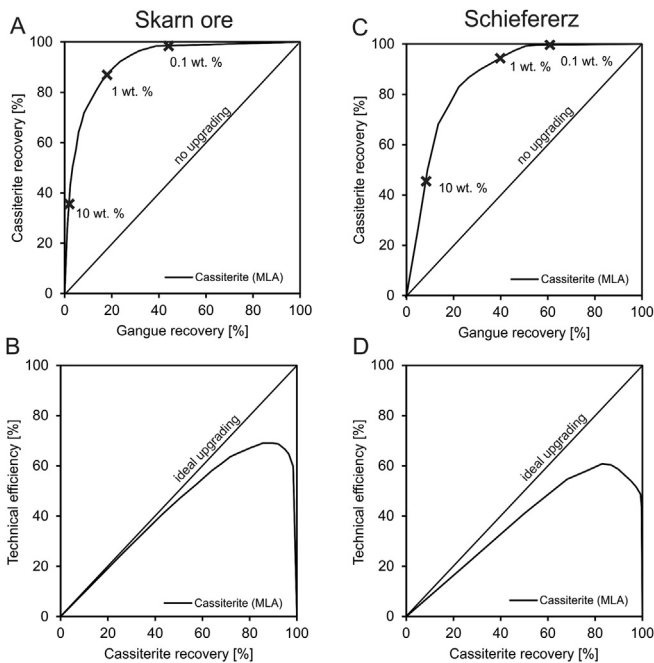
Fig. 5. Upgrading curves based on the sorting parameter cassiterite content [wt %] as determined by MLA. Cassiterite recovery [%] vs. gangue recovery [%] of skarn ore (A) and Schiefererz (C). Technical efficiency [%] vs. cassiterite recovery [%] of skarn ore (B) and Schiefererz (D).
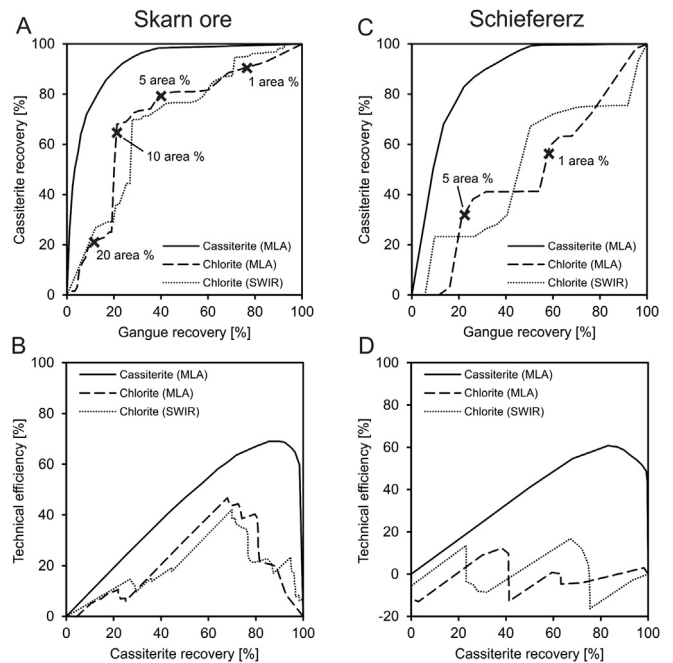
Fig. 6. Upgrading curves based on the sorting parameter chlorite area [%] as determined by MLA and SWIR. The upgrading curve for cassiterite content [wt %] as determined by MLA is shown as a reference. Cassiterite recovery [%] vs. gangue recovery [%] of skarn ore (A) and Schiefererz (C). Technical efficiency [%] vs. cassiterite recovery [%] of skarn ore (B) and Schiefererz (D).
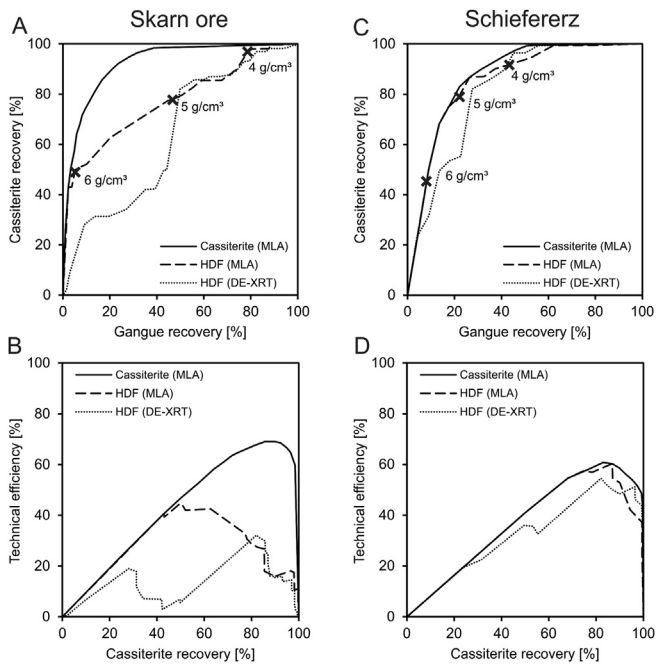
Fig. 7. Upgrading curves based on the sorting parameter highest-density frame [g/cm³] as determined by MLA and DE-XRT. The upgrading curve for cassiterite content [wt %] as determined by MLA is shown as a reference. Cassiterite recovery [%] vs. gangue recovery [%] of skarn ore (A) and Schiefererz (C). Technical efficiency [%] vs. cassiterite recovery [%] of skarn ore (B) and Schiefererz (D).
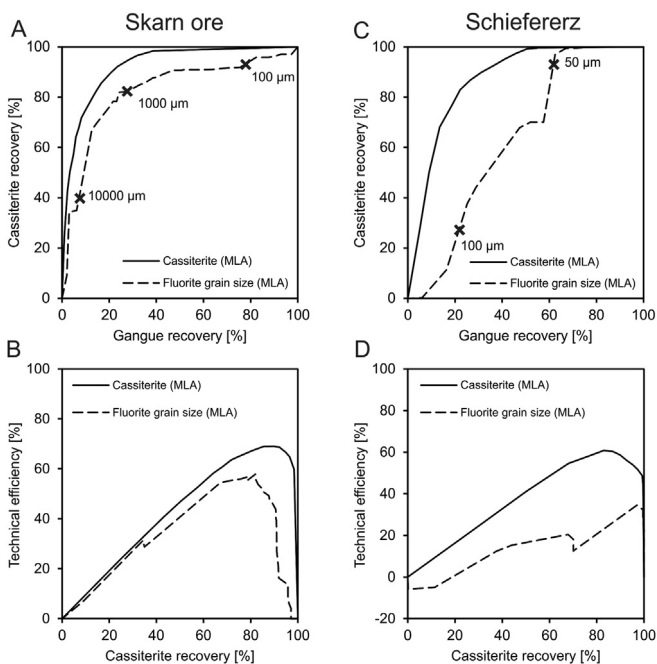
Fig. 8. Upgrading curves based on the sorting parameter fluorite grain size [µm] as determined by MLA. The upgrading curve for cassiterite content [wt %] as determined by MLA is shown as a reference. Cassiterite recovery [%] vs. gangue recovery [%] of skarn ore (A) and Schiefererz (C). Technical efficiency [%] vs. cassiterite recovery [%] of skarn ore (B) and Schiefererz (D).

simulations and poor correlation with sensor data (Fig. 6 C and D).

3.2.3. Highest-density frame

The Fürstenau-II diagram for sorting cassiterite in skarn ore by

the highest-density frame (HDF) is presented in Fig. 7 A. The upgrading curve from sorting with DE-XRT has a significantly lower recovery compared to MLA for HDF values < 5 g/cm³. At this value, approximately 80 % cassiterite recovery and 50% gangue recovery at 30 % technical efficiency can be reached (Fig. 7 A and B).

The upgrading curves from Schiefererz approximate the mineralogical barrier (Fig. 7 C and D). It is possible to recover 95 % cassiterite while rejecting more than 45 % of gangue at a technical efficiency of ~ 50 %. The high density of cassiterite is a distinct property that can be used to efficiently separate cassiterite-bearing mica schist from barren mica schist.

3.2.4. Fluorite grain size

Upgrading curves for sorting by fluorite grain size are shown in Fig. 8. The property grain size was chosen instead of the area because of low median fluorite concentrations (0.1 wt % in skarn ore; 0.5 wt % in Schiefererz). The sorting result for skarn ore is excellent - cassiterite recovery of nearly 80 % at less than 25 % gangue recovery and a technical efficiency of 57 % can be realized. 100 % cassiterite from the Schiefererz can be recovered while rejecting 80 % of the gangue.

However, preliminary test work with a sensor detecting UV-induced fluorescence at 365 nm was not successful. Despite fluorescence being detectable for coarse-grained fluorite, the method did not show reliable identification of fluorite grains <2 mm. Reaching cassiterite recovery of 90 % in skarn ore and Schiefererz would require the identification of fluorite grains as small as 100 µm and 50 µm, respectively.

3.3. Empirical validation

Integration of sensor-based sorting into the beneficiation circuit of a commercial mining operation requires a cost-benefit analysis. Parameters that are typically considered are the recovery of the mineral of interest as well as the technical efficiency. Here, we show that the available MLA data set can play a major role in such an evaluation. It can be used to review the economic potential of sorting and help judging the further processing behavior of the material. The separation of particles from the concentrate stream results in a change of important parameters (like modal mineralogy and mineral grain size) that affect the succeeding beneficiation processes (e.g. comminution, froth flotation, density separation and magnetic separation). The multitude of capabilities for data evaluation is demonstrated by simulating these parameters for the emerging concentrate and waste streams.

As an example, we simulate the separation by two proxies that show promising results from MLA and sensor data: (1) The sorting of skarn ore by using abundance of chlorite as a proxy; (2) The separation of Schiefererz by using the frame with the highest density as a proxy. Modal mineralogy (depending on mass pull), cassiterite grade and average cassiterite grain size (50 wt % passing) of concentrate and waste are modeled for cassiterite recovery classes in 10 % incremental steps. Data can be found in the electronic supplementary (Table 3. Sorted ore).

3.3.1. Skarn ore sorted by chlorite area

With increasing cassiterite recovery, the modal mineralogy of the concentrate is dominated by quartz, chlorite and iron oxide minerals. Fluorite and sulfide minerals preferably accumulate in the concentrate as well (Fig. 9 A). Garnet, epidote and amphibole predominantly report to the waste fraction (Fig. 9 B). Efficient separation between concentrate and waste is possible around approximately 80 % cassiterite recovery, where the cassiterite grade is around 1.2 wt % (Fig. 9 C) at an average grain size of nearly 300 µm (Fig. 9 D). The mass pull into the concentrate at 80 % cassiterite
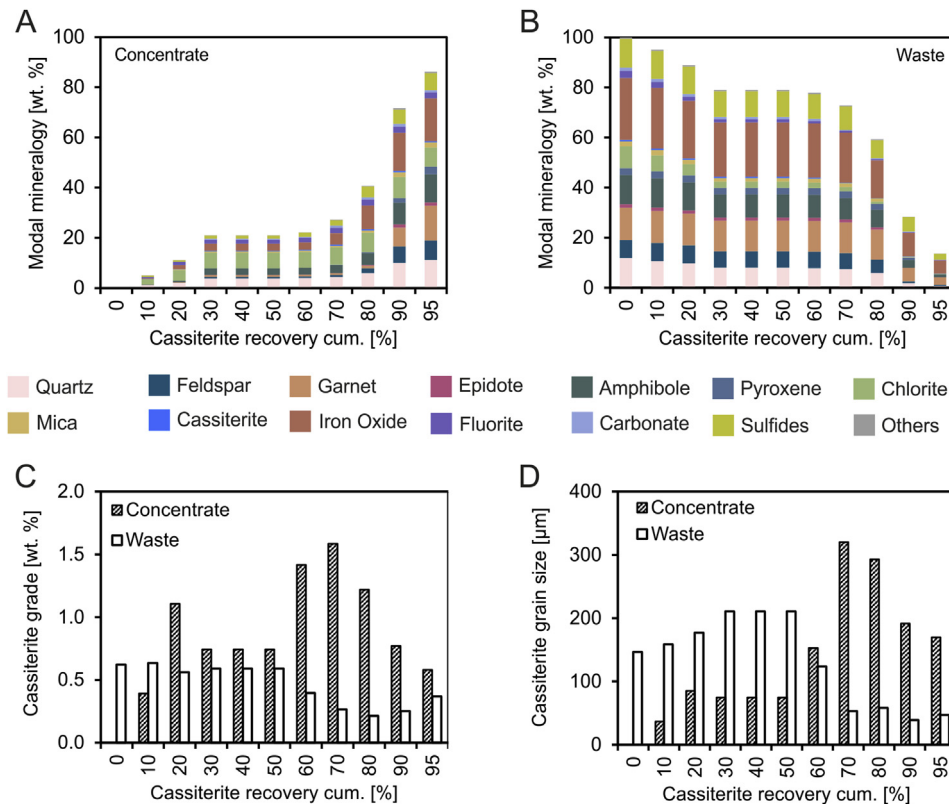
Fig. 9. Cassiterite recovery classes of skarn ore sorted by chlorite area. A. Modal mineralogy of concentrate. B. Modal mineralogy of waste. C. Cassiterite grade. D. Cassiterite grain size.

recovery is only 40 %. The average cassiterite grain size in the waste stream is below 60 μm. Thorough grinding will be necessary to reach a high degree of liberation for such small grain sizes (Buchmann et al., 2018). In the 90 % cassiterite recovery class, the concentrate is diluted with garnet and amphibole which increases the mass pull above 70 wt %. Achieving a cassiterite recovery of 10 % more would hence require a beneficiation plant that allows 75 % higher throughput. Lower cassiterite grade (0.8 wt %) and average cassiterite grain sizes (<200 μm) are other tangible variables that deteriorate the properties of the concentrate for a higher cassiterite recovery. Considering all parameters presented the threshold value for most efficient skarn ore separation lies thus between 80 and 90 % cassiterite recovery.

3.3.2. Schiefererz sorted by highest-density frame

The separation of the Schiefererz shows a dominance of quartz in the concentrate and feldspar and mica in the waste stream. In comparison to the skarn ore, the modal mineralogy barely changes and will have only limited effects for downstream beneficiation processes. Recovery of 50 % cassiterite is achieved by concentrating only the two samples with the highest cassiterite contents (i.e. highest-density frames). 95 % of the cassiterite can be recovered with 50 % mass pull (Fig. 10 A and B). The average cassiterite grain size in this concentrate would be > 1500 μm (Fig. 10 D) at a grade of 3.62 % (Fig. 10 C). Contrary to the skarn ore, the average cassiterite grain size in the waste stream still exceeds 200 μm. Particles containing such coarse-grained cassiterite are still valuable and should be targeted in sorting. Taking into account all available information suggests that a cassiterite recovery above 95 % should be the target of an efficient beneficiation route for the Schiefererz.

4. Discussion

Results illustrate an excellent correspondence between empirical test results and simulations of separation performance based on MLA data. The properties of minerals in the ore (modal mineralogy, mineral density, mineral grain size, etc.) can be used to predict the separation success of different ore types and allow preparing a detailed cost-benefit analysis and making an educated choice for the best-suited sensor. Once a sensor is chosen, acquired data can also serve for optimization of the sorting process itself. The properties of minerals in the simulated concentrate can be used to plan and predict the functionality of following processes like froth flotation, density separation and magnetic separation and to determine the decreased toxicity of coarse-grained waste. Accordingly, the simulation of sensor-based sorting should become a fundamental component of a predictive geometallurgical model that integrates the entire beneficiation process from comminution to purification (van den Boogaart and Tolosana Delgado, 2018).

Sorting skarn ore by chlorite abundance is a good example for the interactions between sensor-based sorting and subsequent processing steps: The unavoidable high amount of chlorite in the concentrate is disadvantageous for further processing, as chlorite readily responds to reagents that are used in cassiterite flotation. This may, of course complicate the separation of the two minerals (Bulatovic, 2010). The simulated composition of the concentrate (here most importantly chlorite abundance and cassiterite abundance) and other properties (e.g., intergrowth between the two minerals) are important factors that modify the process of froth flotation (which can be simulated as well; e.g., Lamberg and Vianna (2007); van den Boogaart and Tolosana Delgado (2018)). Furthermore, the modified composition of the ore affects subsequent density separation and magnetic separation, which must be taken
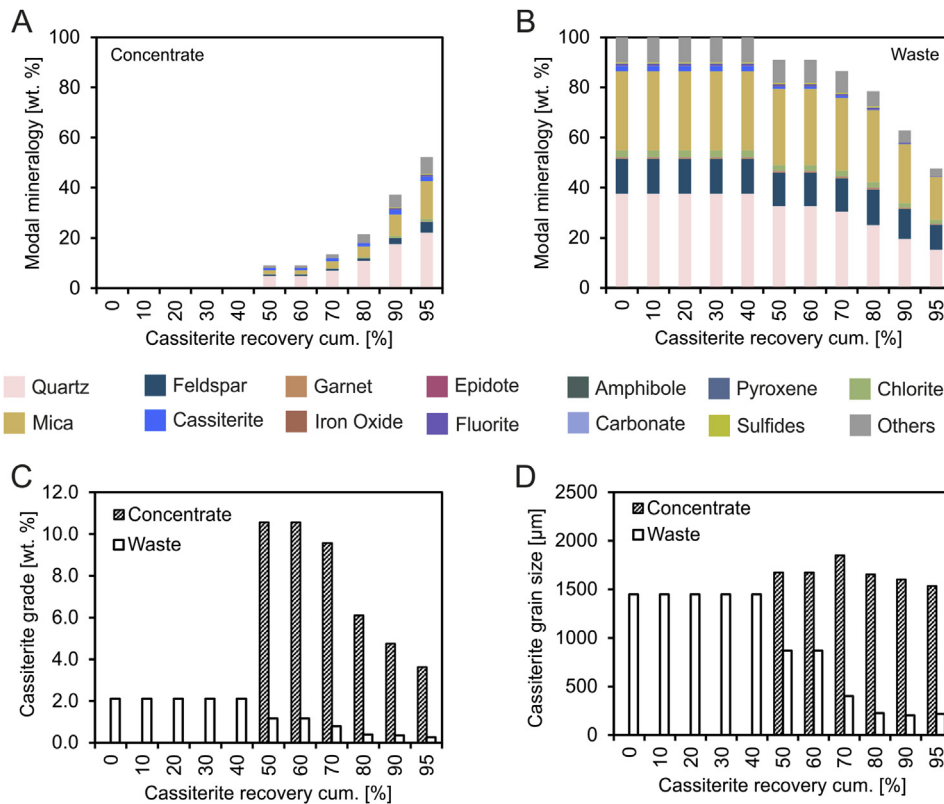
Fig. 10. Cassiterite recovery classes of Schiefererz sorted by HDF. A. Modal mineralogy of concentrate. B. Modal mineralogy of waste. C. Cassiterite grade. D. Cassiterite grain size.

into consideration in models that predict the separation behavior of the ore (e.g., Buchmann et al., 2017; Hannula et al., 2018).

There are two main reasons for the poor correlation between DE-XRT values and HDF values (from MLA) > 5 g/cm³ in the skarn samples: (1) the cassiterite grains (5 μm–3 mm) are smaller than the resolution of the DE-XRT sensor (3.5 mm pixel width) and (2) the presence of other dense minerals such as magnetite, hematite and sulfide minerals. The frame with the highest density reaches high values for samples containing high contents of iron oxide minerals ($\rho \sim 5$ g/cm³) and/or sulfide (ρ between 4.5 and 7.5 g/cm³). Compared to that, samples with cassiterite in a matrix of minerals with a low density (e.g. chlorite, fluorite, quartz) have a lower HDF value. Correlation between both methods exists only for samples with a HDF <5 g/cm³ (silicate and silicate-cassiterite dominated samples). Better correlation is expected to be reached by a DE-XRT sensor with higher lateral resolution. A discrepancy in lateral resolution also exists between MLA and the SWIR measurements (1.7 mm lateral resolution). Slight deviations in the quantification of relevant parameters result in a slightly changed order of particles in the simulation. This difference does, however, not affect the overall agreement.

Simulation data presented in this study is based on analysis with MLA but data sets of equal quality can also be obtained with similar SEM-EDS-based platforms like TIMA-X (TESCAN, Brno, Czech Republic), Mineralogic Mining (Zeiss, Oberkochen, Germany), and QEMSCAN (FEI Company, Hillsboro, OR, USA). These systems all have in common that analyses are rather time-consuming and costly, especially at the very high degree of spatial resolution that was applied for this study. There are several possibilities to reduce both cost and time, thereby making the simulation-based approach more interesting to be applied by industry. For instance, the resolution of SEM-EDS platforms can be lowered to a level of detail where it still sufficiently characterizes the major minerals and ore

minerals of a sample and allows simulating the separation process. This will speed up the analysis and thus also reduce costs. It is also possible to analyze samples with other technologies that allow spatial analysis at high resolution in shorter time. Examples include mapping by μ-EDXRF and LIBS (e.g., Kuhn et al., 2016; Nikonow et al., 2019). For less complex ores, optical microscopy-based image analysis (e.g. Berrezueta et al., 2016) may well be used to substitute SEM-EDS.

5. Conclusions

The simulation-based approach introduced here enables integral optimization of major parameters that are relevant for sensor-based sorting whilst minimizing the need of time-consuming empirical test work. Quantitative mineralogical and mineral association data can be used to run an unlimited number of sorting simulations, which helps finding proxies for ore sorting and allows choosing a sensor suitable for most efficient separation of coarse-grained particles. Parameters like modal mineralogy, mineral associations and mineral grain size distribution of the simulated products (concentrate and waste) can be anticipated from the data - information that is also of great significance for further minerals beneficiation processes. In combination, this information can contribute significantly to any predictive geometallurgical study (van den Boogaart and Tolosana Delgado, 2018). The approach can be adapted for many other ore types and has a great potential to become a key technology for optimization within the mineral beneficiation industry if the cost for this type of analysis can be lowered.

Declarations of interest

None.

Acknowledgements

Appendix A. Supplementary data

Supplementary data to this article can be found online at https://doi.org/10.1016/j.jclepro.2019.06.259.

References

Bauer, M.E., Seifert, T., Burisch, M., Krause, J., Richter, N., Gutzmer, J., 2017. Indium-bearing sulfides from the Hämmerlein skarn deposit, Erzgebirge, Germany: evidence for late-stage diffusion of indium into sphalerite. Miner. Depos. https://doi.org/10.1007/s00126-017-0773-1.

Berrezueta, E., Ordóñez-Casado, B., Bonilla, W., Banda, R., Castroviejo, R., Carrión, P., Puglla, S., 2016. Ore petrography using optical image analysis: application to zaruma-portovelo deposit (Ecuador). Geosciences 6 (2), 30.

Buchmann, M., Leißner, T., Kern, M., Schach, E., Tolosana-Delgado, R., Rudolph, M., Gutzmer, J., Peuker, U.A., 2018. Fine Grinding Characteristics of Cassiterite-Bearing Skarn Ore. European Mineral Processing and Recycling Congress, Essen, Germany.

Buchmann, M., Schach, E., Bremerstein, I., Astoveza, J., Kern, M., Leißner, T., Peuker, U.A., Rudolph, M., 2017. Flotation characteristics of a cassiterite bearing complex skarn ore from the Ore Mountains. In: Germany, Flotation '17 Conference. Cape Town, South Africa.

Bulatovic, S.M., 2010. Handbook of Flotation Reagents Vol. II: Chemistry, Theory and Practice: Flotation of Gold, PGM and Oxide Minerals. Elsevier, Amsterdam.

Dalm, M., Buxton, M.W.N., van Ruitenbeek, F.J.A., 2017. Discriminating ore and waste in a porphyry copper deposit using short-wavelength infrared (SWIR) hyperspectral imagery. Miner. Eng. 105, 10–18.

Drzymała, J., 2006. Atlas of upgrading curves used in separation and mineral science and technology. Physicochemical Problems of Mineral Processing 40 (1), 19–29.

Drzymała, J., 2007. Atlas of upgrading curves used in separation and mineral science and technology. Part II. Physicochemical Problems of Mineral Processing 41 (1), 27–35.

Drzymała, J., 2008. Atlas of upgrading curves used in separation and mineral science and technology. Part III. Physicochemical Problems of Mineral Processing 42 (1), 75–84.

Fandrich, R., Gu, Y., Burrows, D., Moeller, K., 2007. Modern SEM-based mineral liberation analysis. Int. J. Miner. Process. 84 (1–4), 310–320.

Finch, J.A., Gomez, C.O., 1989. Separability curves from image analysis data. Miner. Eng. 2 (4), 565–568.

Gu, Y., 2003. Automated scanning electron microscope based mineral liberation analysis an introduction to JKMRC/FEI mineral liberation analyser. J. Miner. Mater. Charact. Eng. 2 (1), 33–41.

Hannula, J., Kern, M., Luukkanen, S., Roine, A., van den Boogaart, K.G., Reuter, M.A., 2018. Property-based modelling and simulation of mechanical separation processes using dynamic binning and neural networks. Miner. Eng. 126, 52–63.

Iyakwari, S., Glass, H.J., Kowalczuk, P.B., 2013. Potential for near infrared sensor-based sorting of hydrothermally-formed minerals. J. Near Infrared Spectrosc. 21 (3), 223–229.

Jakob, S., Zimmermann, R., Gloaguen, R., 2017. The need for accurate geometric and radiometric corrections of drone-borne hyperspectral data for mineral exploration: MEPHySTo—a toolbox for pre-processing drone-borne hyperspectral data. Rem. Sens. 9 (1), 88.

Kästner, J., 2016. Detailed Investigations of Skarn Lithologies and Tin Mineralisation of the Hämmerlein Seam (+590 m level) in the Pöhla Tellerhäuser ore district. M.Sc. Thesis. Institute for Mineralogy, Technical University Bergakademie Freiberg, Freiberg, p. 144.

Kern, M., Kästner, J., Tolosana-Delgado, R., Jeske, T., Gutzmer, J., 2018a. The inherent link between ore formation and geometallurgy as documented by complex tin mineralization at the Hämmerlein deposit (Erzgebirge, Germany). Miner. Depos. https://doi.org/10.1007/s00126-018-0832-2.

Kern, M., Möckel, R., Krause, J., Teichmann, J., Gutzmer, J., 2018b. Calculating the deportment of a fine-grained and compositionally complex Sn skarn with a modified approach for automated mineralogy. Miner. Eng. 116, 213–225.

Knapp, H., Neubert, K., Schropp, C., Wotruba, H., 2014. Viable applications of sensor-based sorting for the processing of mineral resources. Chem. Ing. Tech. 86 (6), 773–783.

Krupko, N., Kern, M., Schach, E., Buchmann, M., Bremerstein, I., van den Boogaart, K.G., 2018. MLALookUP — a new software for geometallurgical and process-oriented analysis of MLA data. In: Resources for Future Generations 2018 Conference. Vancouver, Canada.

Kuhn, K., Meima, J.A., Rammlmair, D., Ohlendorf, C., 2016. Chemical mapping of mine waste drill cores with laser-induced breakdown spectroscopy (LIBS) and energy dispersive X-ray fluorescence (EDXRF) for mineral resource exploration. J. Geochem. Explor. 161, 72–84.

Lamberg, P., Vianna, S., 2007. A technique for tracking multiphase mineral particles in flotation circuits. In: XXII Encontro Nacional de Tratamento de Minérios e Metalurgia Extrativa/VIII Meeting of the Southern Hemisphere on Mineral Technology. Ouro Preto, Brazil.

Miehlbradt, M., 2017. Mapping and Mineral-Chemical Characterization of the Tin-Bearing Mineralization from the "Schist Ore" Type of the Sn-Polymetallic Deposit Hämmerlein, Distric Pöhla, Germany, Institute for Mineralogy. M.Sc. Thesis. Technical University Bergakademie Freiberg, Freiberg, p. 85.

Nadolski, S., Samuels, M., Klein, B., Hart, C.J.R., 2018. Evaluation of bulk and particle sensor-based sorting systems for the New Afton block caving operation. Miner. Eng. 121, 169–179.

Neubert, K., Wotruba, H., 2016. Investigations on the detectability of rare-earth minerals using dual-energy X-ray transmission sorting. Journal of Sustainable Metallurgy 3 (1), 3–12.

Nienhaus, K., Pretz, T., Wotruba, H., 2014. Sensor Technologies: Impluses for the Raw Materials Industry. Schriftenreihe zur Aufbereitung und Veredlung (Band 50). Shaker Verlag, Aachen.

Nikonow, W., Rammlmair, D., Meima, J.A., Schodlok, M.C., 2019. Advanced mineral characterization and petrographic analysis by μ-EDXRF, LIBS, HSI and hyperspectral data merging. Mineral. Petrol. 113 (3), 417–431.

Phiri, T., Glass, H.J., Mwamba, P., 2018. Development of a strategy and interpretation of the NIR spectra for application in automated sorting. Miner. Eng. 127, 224–231.

Pontual, S., Merry, N., Gamson, P., 1997. Spectral Interpretation Field Manual. Spectral Analysis Guides for Mineral Exploration, vol. 1. AusSpec International Pty. Ltd., Victoria, Australia.

Richter, N., 2016. Indium-bearing Sulfides and Associated Minerals from the Poly-metallic Skarn Deposit Pöhla-Hämmerlein, Western Erzgebirge, Germany. M.Sc. Thesis. Institute of Mineralogy. Technische Universität Bergakademie Freiberg, Germany, p. 184.

Riedel, F., Dehler, M., 2010. Recovery of unliberated diamonds by x-ray transmission sorting. In: Diamonds - Source to Use 2010 Conference. Gaborone, Botswana.

Robben, M.R., Knapp, H., Dehler, M., Wotruba, H., 2013. X-ray transmission sorting of tungsten ore. In: Optical Characterization of Materials Conference. Karlsruhe, Germany.

Schuppan, W., Hiller, A., 2012. Die Komplexlagerstätten Tellerhäuser und Hämmerlein. Bergbaumonographie. Bergbau in Sachsen (Band 17). In: Sächsisches Landesamt für Umwelt und Geologie, Sächsisches Oberbergamt, Freiberg.

Treliver Minerals Limited, 2015. Tellerhäuser Project Resource Statement. Press Release. http://www.anglosaxony.com/assets/file/Press%20Release%20Mar%202015.pdf. (Accessed 9 July 2018).

van den Boogaart, K.G., Tolosana Delgado, R., 2018. Predicitve geometallurgy: an interdisciplinary key challenge for mathematical geosciences. In: Sagar, B.S.D., Cheng, Q., Agterberg, F. (Eds.), Handbook of Mathematical Geosciences. Springer, Cham.

von Ketelhodt, L., Bergmann, C., 2010. Dual Energy X-ray transmission sorting of coal. J. S. Afr. Inst. Min. Metall 110, 371–378.

Walker, S., 2017. Squeezing the stone. Eng. Min. J. 44–51. Dec 2017.

Wills, B.A., Finch, J.A., 2016. Wills' Mineral Processing Technology. An Introduction to the Practical Aspects of Ore Treatment and Mineral Recovery, 8 ed. Elsevier, Amsterdam.

Winkler, C., 2017. Petrographische und geochemische Charakterisierung der Nebengesteinsalteration im unmittelbaren Kontakt zum Hammerlein Skarn, Institute for Mineralogy. B.Sc. Thesis. Technical University Bergakademie Freiberg, Freiberg, p. 71.

Wotruba, H., Harbeck, H., 2010. Sensor-based sorting. In: Elvers, B. (Ed.), Ullmann's Encyclopedia of Industrial Chemistry. John Wiley and Sons, Weinheim.